

## **Supporting Information**

### **Free-standing quaternized cellulose-based paper cathode enabling high-performance zinc-iodine batteries**

Qian Zhang, Dong Han, Jinwang Ma, Bingyi Liu, Guijuan Wei,\* and Xixia Zhao\*

State Key Laboratory of Green Papermaking and Resource Recycling, Faculty of  
Light Industry, Qilu University of Technology (Shandong Academy of Sciences),  
Jinan, 250353, P. R. China

\*Corresponding author

E-mail: zhaoxixia163@163.com; weitiansd@126.com

## **Experimental section**

### **Preparation of cellulose dispersion**

Cellulose pulp boards were first immersed in deionized water and soaked overnight to ensure complete wetting. The swollen pulp was then mechanically disintegrated to obtain a homogeneous cellulose dispersion with a solid content of 5 wt%.

### **Preparation of quaternized cellulose dispersion**

A 5 wt% NaOH aqueous solution was prepared and used for the alkaline pretreatment of the cellulose slurry. Subsequently, 2,3-epoxypropyltrimethylammonium chloride (EPTAC) was added, with the molar ratio of EPTAC to anhydroglucose units in cellulose ( $n_{\text{EPTAC}}/n_{\text{AGU}}$ ) set to 0 or 10. The mixture was thoroughly stirred, transferred into a three-neck round-bottom flask, and allowed to react at 65 °C for 8 h. After completion of the reaction, the mixture was neutralized with dilute hydrochloric acid, followed by filtration and repeated washing with deionized water until no  $\text{Cl}^-$  ions were detected in the filtrate.

### **Fabrication of quaternized cellulose conductive paper**

The quaternized cellulose dispersion was diluted to the desired concentration, after which carbon nanotubes (CNTs) were added. The mass ratio of quaternized cellulose fibers to CNTs was 6:4. The mixture was subjected to ultrasonic treatment for 30 min to ensure uniform dispersion of CNTs and intimate mixing with the cellulose matrix. The resulting suspension was divided into two equal portions and vacuum-filtered using polypropylene microporous membranes. The obtained paper electrodes were dried in an oven at 60 °C for more than 24 h to ensure complete removal of residual moisture. After cooling to room temperature, the dried papers were punched into circular disks with a diameter of 12 mm. According to the  $n_{\text{EPTAC}}/n_{\text{AGU}}$  ratio, the resulting conductive papers were denoted as CF/CNTs (without quaternization) and EPTAC-CF/CNTs (with quaternization).

### **Fabrication of iodine cathodes**

An iodine solution was prepared by dissolving 0.37 g of  $\text{I}_2$  and 0.74 g of KI in 10 g of deionized water under stirring until complete dissolution. Prior to battery assembly,

iodine cathodes were prepared by drop-casting 10  $\mu\text{L}$  of the iodine solution onto the surface of the conductive paper substrates, with the loading amount controlled at 0.76  $\text{mg cm}^{-2}$ . According to the  $n_{\text{EPTAC}}/n_{\text{AGU}}$  ratio, the obtained iodine-loaded cathodes were denoted as CF/CNTs@I and EPTAC-CF/CNTs@I, respectively.

### **Assembly of zinc-iodine batteries**

CR2032-type coin cells were assembled using as-prepared cathodes in ambient atmosphere. The electrolyte is 200  $\mu\text{L}$  of 2 M  $\text{ZnSO}_4$  aqueous solution. A Whatman GF/D glass fiber separator with a diameter of 19 mm was employed, and the zinc foil anode had a thickness of 0.3 mm.

### **Characterization**

Phase identification of the samples was carried out using an X-ray diffractometer (XRD, Rigaku SmartLab) equipped with  $\text{Cu K}\alpha$  radiation ( $\lambda = 1.5406 \text{ \AA}$ ), operated at 40 kV and 40 mA. The diffraction patterns were recorded over a  $2\theta$  range of  $5^\circ$ - $60^\circ$ . The surface morphology of the samples was examined using a scanning electron microscope (SEM, Regulus 8220) operated at an accelerating voltage of 5 kV. Prior to SEM observation, all samples were sputter-coated with a thin layer of gold to improve electrical conductivity. Elemental distribution analysis was performed using an energy-dispersive X-ray spectroscopy (EDS) system attached to the SEM. Fourier transform infrared (FT-IR) spectra were collected on a Bruker ALPHA spectrometer using the attenuated total reflectance (ATR) mode over the wavenumber range of  $400$ – $4000 \text{ cm}^{-1}$  with a resolution of  $4 \text{ cm}^{-1}$  to identify the functional groups of the materials. X-ray photoelectron spectroscopy (XPS) measurements were conducted using an Escalab Xi<sup>+</sup> system (Thermo Fisher Scientific, USA) with a monochromatic  $\text{Al K}\alpha$  radiation source.

### **Electrochemical testing**

Galvanostatic charge-discharge (GCD) measurements were carried out using a Neware battery testing system to evaluate the cycling performance and rate capability of the assembled cells. All tests were conducted within a voltage window of 0.6-1.6 V at a controlled temperature of 25  $^\circ\text{C}$  using a constant-temperature chamber.

Cyclic voltammetry (CV) and electrochemical impedance spectroscopy (EIS) measurements were performed on a CHI 760E electrochemical workstation (Shanghai Chenhua, China). The CV tests were conducted over a potential range of 0.6-1.6 V. EIS measurements were carried out under open-circuit conditions over a suitable frequency range (unless otherwise specified).

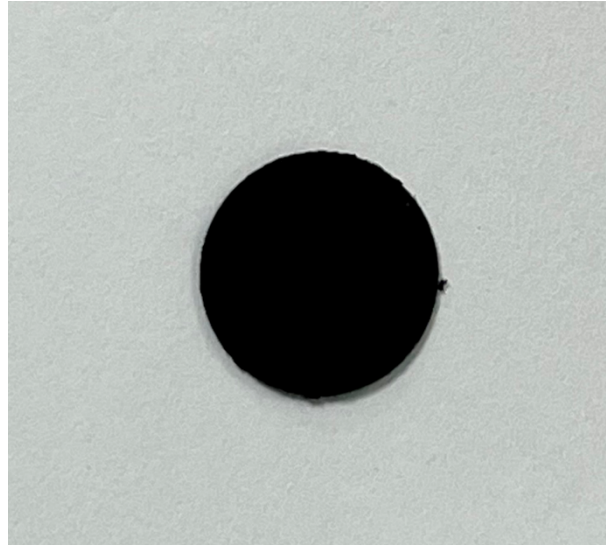


**Fig. S1** Photo of the EPTAC-CF/CNTs conductive paper.

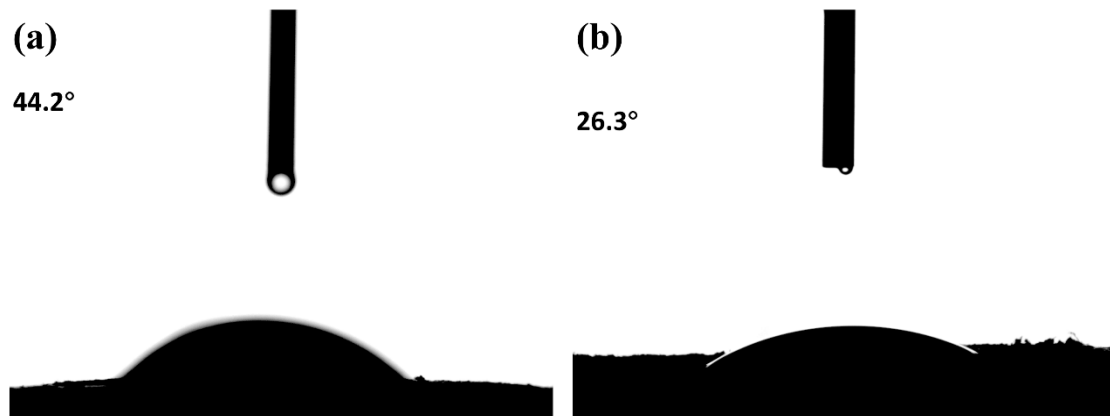


**Fig. S2** Contact angles of (a) CF/CNTs and (b) EPTAC-CF/CNTs.

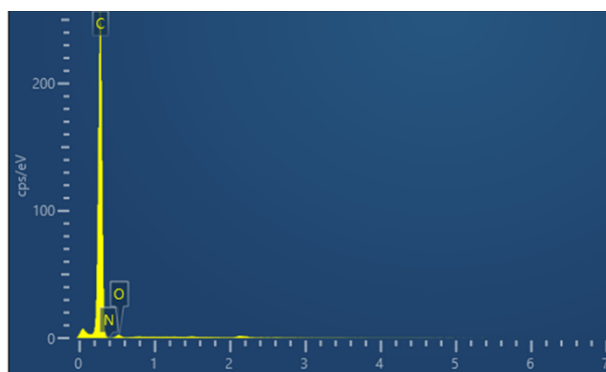


**Fig. S3** EDS profile of EPTAC-CF/CNTs.

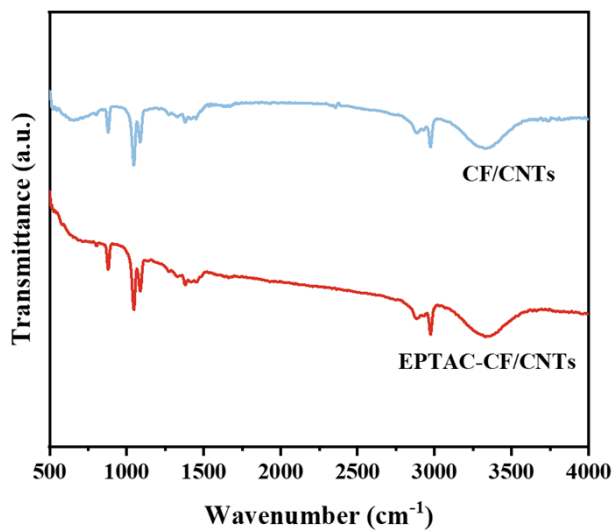


**Fig. S4** FT-IR spectra of CF/CNTs and EPTAC-CF/CNTs.

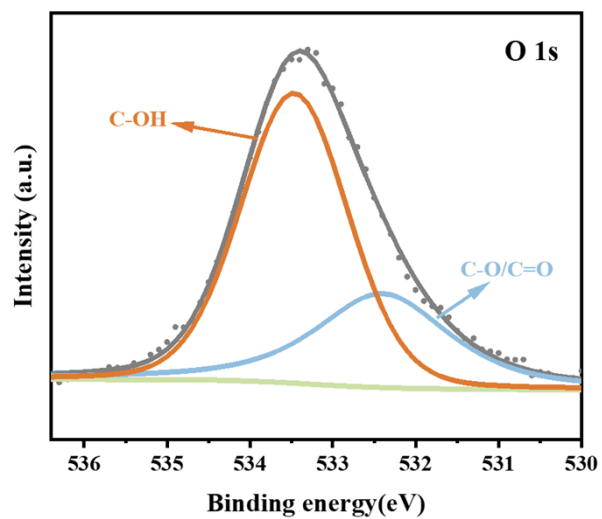


**Fig. S5** High-resolution O 1s XPS spectrum of CF/CNTs.

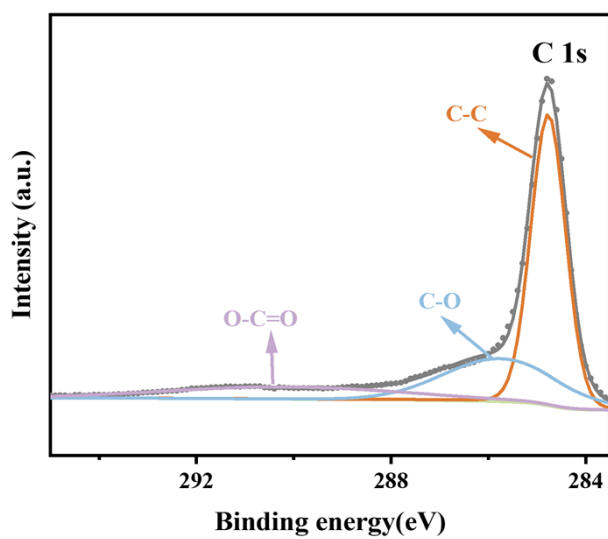


**Fig. S6** High-resolution C 1s XPS spectrum of CF/CNTs.

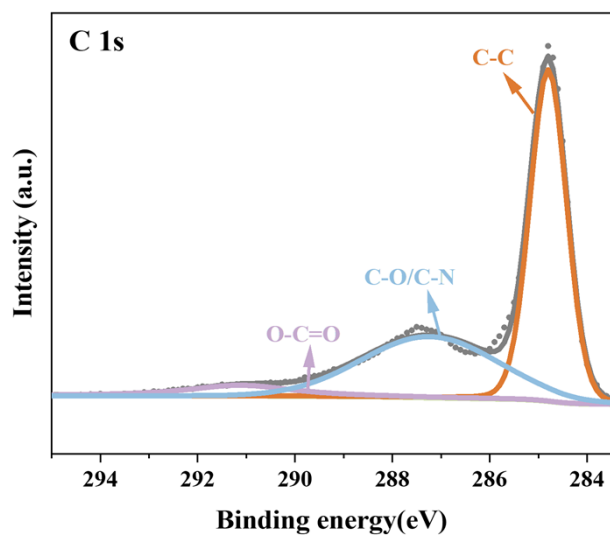


**Fig. S7** High-resolution C 1s XPS spectrum of EPTAC-CF/CNTs.

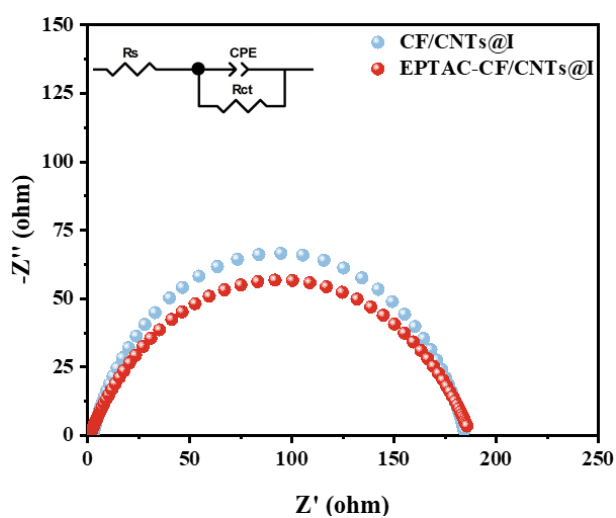


**Fig. S8** Fitted EIS Nyquist plots and corresponding equivalent circuit of CF/CNTs@I and EPTAC-CF/CNTs@I electrodes.

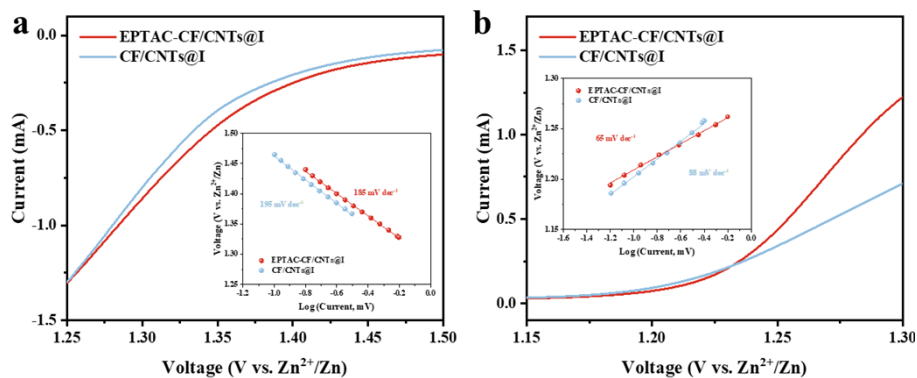


**Fig. S9** (a,b) Tafel plots and corresponding Tafel slopes of CF/CNTs@I and EPTAC-CF/CNTs@I cathodes.

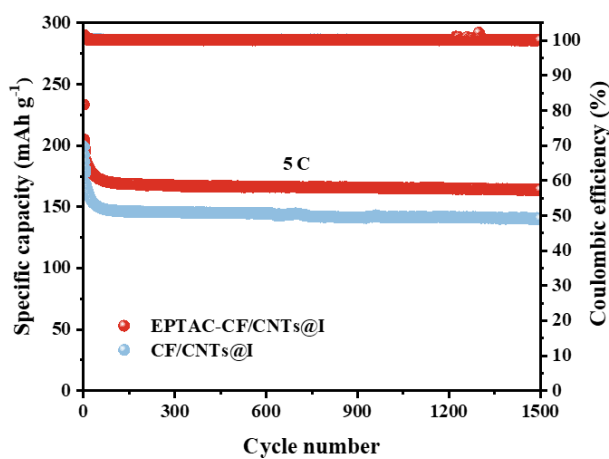


**Fig. S10** Long-term cycling performance of CF/CNTs@I and EPTAC-CF/CNTs@I cathodes at 5 C.

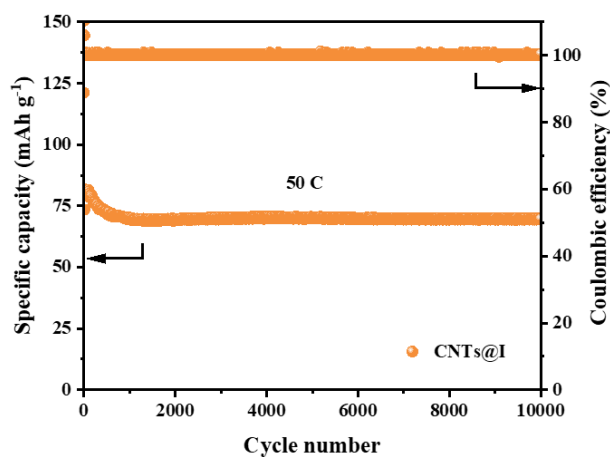


**Fig. S11** Cycling performance of the CNT@I cathode at 50 C.

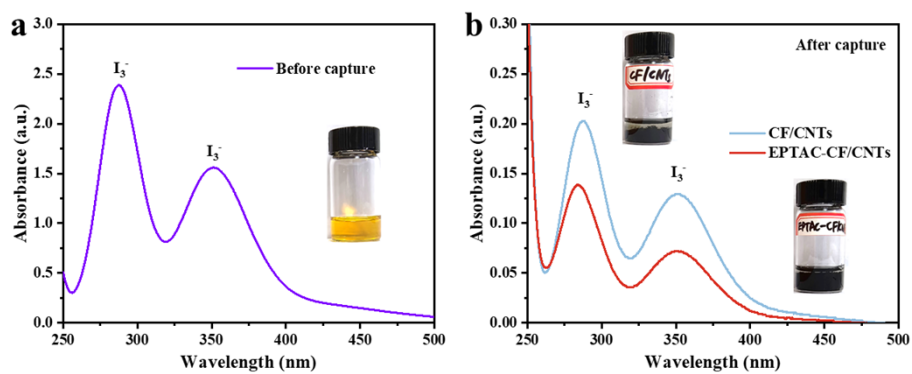


**Fig. S12** (a) UV-vis absorption spectrum of the pristine iodine solution before adsorption. (b) UV-vis absorption spectra of iodine solutions after adsorbed by CF/CNTs and EPTAC-CF/CNTs.